

RESEARCH ARTICLE

MRI-based visualization of rTMS-induced cortical plasticity in the primary motor cortex

Kaori Tamura¹, Takahiro Osada¹, Akitoshi Ogawa¹, Masaki Tanaka¹, Akimitsu Suda^{1,2}, Yasushi Shimo², Nobutaka Hattori², Koji Kamagata³, Masaaki Hori³, Shigeki Aoki³, Takahiro Shimizu⁴, Hiroyuki Enomoto⁵, Ritsuko Hanajima⁴, Yoshikazu Ugawa⁵, Seiki Konishi^{1,6,7,8*}

1 Department of Neurophysiology, Juntendo University School of Medicine, Tokyo, Japan, **2** Department of Neurology, Juntendo University School of Medicine, Tokyo, Japan, **3** Department of Radiology, Juntendo University School of Medicine, Tokyo, Japan, **4** Department of Neurology, Tottori University School of Medicine, Tottori, Japan, **5** Department of Neuro-Regeneration, Fukushima Medical University, Fukushima, Japan, **6** Research Institute for Diseases of Old Age, Juntendo University School of Medicine, Tokyo, Japan, **7** Sportology Center, Juntendo University School of Medicine, Tokyo, Japan, **8** Advanced Research Institute for Health Science, Juntendo University School of Medicine, Tokyo, Japan

☯ These authors contributed equally to this work.

* skonishi@juntendo.ac.jp



OPEN ACCESS

Citation: Tamura K, Osada T, Ogawa A, Tanaka M, Suda A, Shimo Y, et al. (2019) MRI-based visualization of rTMS-induced cortical plasticity in the primary motor cortex. PLoS ONE 14(10): e0224175. <https://doi.org/10.1371/journal.pone.0224175>

Editor: Bernadette Ann Murphy, University of Ontario Institute of Technology, CANADA

Received: May 24, 2019

Accepted: October 6, 2019

Published: October 24, 2019

Copyright: © 2019 Tamura et al. This is an open access article distributed under the terms of the [Creative Commons Attribution License](https://creativecommons.org/licenses/by/4.0/), which permits unrestricted use, distribution, and reproduction in any medium, provided the original author and source are credited.

Data Availability Statement: All data are available at Dryad "Data from: MRI-based visualization of rTMS-induced cortical plasticity in the primary motor cortex" (doi:[10.5061/dryad.fj6q573pw](https://doi.org/10.5061/dryad.fj6q573pw)).

Funding: This work was supported by JSPS KAKENHI (<https://www.jspss.go.jp/>) Grant Number 16K18367 and 18K07348 to T.O. and a grant from Takeda Science Foundation (<https://www.takeda-sci.or.jp/>) to SK. The funders had no role in study design, data collection and analysis, decision to publish, or preparation of the manuscript.

Abstract

Repetitive transcranial magnetic stimulation (rTMS) induces changes in cortical excitability for minutes to hours after the end of intervention. However, it has not been precisely determined to what extent cortical plasticity prevails spatially in the cortex. Recent studies have shown that rTMS induces changes in "interhemispheric" functional connectivity, the resting-state functional connectivity between the stimulated region and the symmetrically corresponding region in the contralateral hemisphere. In the present study, quadripulse stimulation (QPS) was applied to the index finger representation in the left primary motor cortex (M1), while the position of the stimulation coil was constantly monitored by an online navigator. After QPS application, resting-state functional magnetic resonance imaging was performed, and the interhemispheric functional connectivity was compared with that before QPS. A cluster of connectivity changes was observed in the stimulated region in the central sulcus. The cluster was spatially extended approximately 10 mm from the center [half width at half maximum (HWHM): approximately 3 mm] and was extended approximately 20 mm long in depth (HWHM: approximately 7 mm). A localizer scan of the index finger motion confirmed that the cluster of interhemispheric connectivity changes overlapped spatially with the activation related to the index finger motion. These results indicate that cortical plasticity in M1 induced by rTMS was relatively restricted in space and suggest that rTMS can reveal functional dissociation associated with adjacent small areas by inducing neural plasticity in restricted cortical regions.

Introduction

Transcranial magnetic stimulation (TMS) is a non-invasive method to induce neural activity of stimulated regions or block their functions transiently and is also capable of changing

Competing interests: The authors have declared that no competing interests exist.

behavior [1–4]. Since behavioral changes are thought to result primarily from changes in neural activity in the stimulated region and connectivity with other brain regions, it is important to understand the spatial extent of the effect of stimulation that prevails in the stimulated region. Electric field measurements have provided the spatial distribution of field strength in the stimulated region [5–12]. Concurrent measurements using functional magnetic resonance imaging (fMRI) and TMS have also revealed the spatial distribution of MRI signals in local and remote brain regions elicited by magnetic stimulation [13–18]. Repetitive TMS (rTMS), on the other hand, has been used to induce changes in cortical excitability of stimulated regions for minutes to hours after the end of the intervention, which may result in behavioral changes [1–4]. It is also important to understand the spatial extent of cortical plasticity induced by rTMS. However, the visualization of the spatial extent of cortical plasticity remains largely uninvestigated.

Recent MRI studies have investigated the effects of rTMS on functional connectivity and revealed changes in functional connectivity between the stimulated region and other brain regions after rTMS [19–44]. Our previous study has demonstrated changes in “interhemispheric” functional connectivity, the resting-state functional connectivity between the stimulated region and the symmetrically corresponding region in the contralateral hemisphere [33]. It found that, after stimulation to the left primary motor cortex (M1), inhibitory rTMS increased interhemispheric functional connectivity between bilateral M1 while excitatory rTMS decreased it. This previous study employed a region of interest-based analysis in the stimulated region in M1, and suggests that interhemispheric functional connectivity can be utilized to examine the spatial extent of cortical plasticity in the stimulated region by calculating the connectivity in a voxel-by-voxel basis, with no assumption of functional symmetry of the cortex.

In the present study, to examine the spatial extent of cortical plasticity, we measured interhemispheric functional connectivity changes in the first dorsal interosseous (FDI) representation in the M1 in the left hemisphere. Quadripulse stimulation (QPS) [33, 40, 45, 46] was applied to induce changes in cortical excitability in the M1, while the position and orientation of the stimulation coil were constantly monitored by an online navigator. The voxel-wise changes of interhemispheric functional connectivity after QPS were calculated to visualize the spatial extent of cortical plasticity. Localizer scans of the finger movement task were also administered to compare the spatial extent of brain activation in the M1 with that of changes in interhemispheric functional connectivity.

Materials and methods

Subjects

Twenty right-handed subjects [12 men and 8 women, age: 25.9 ± 9.0 years (mean \pm SD) ranging from 20 to 48 years] participated in the experiments. Written informed consent was obtained from all subjects according to the Declaration of Helsinki. The experimental procedures were approved by the Institutional Review Board of Juntendo University School of Medicine.

Overall design of the combined rTMS-fMRI experiment

The experiment consisted of two daily sessions (Fig 1A). On the first day, T1-weighted structural images were acquired. Then, the subjects underwent a resting-state scan for five runs without QPS as a control connectivity scan. On the second day, the motor evoked potential (MEP) was measured to search for the hot spot of the FDI representation in the M1. Then, QPS was delivered to the hot spot for 30 min to induce cortical plasticity at the FDI-M1. An online navigation system was utilized to maintain accurate stimulation onto the hot spot

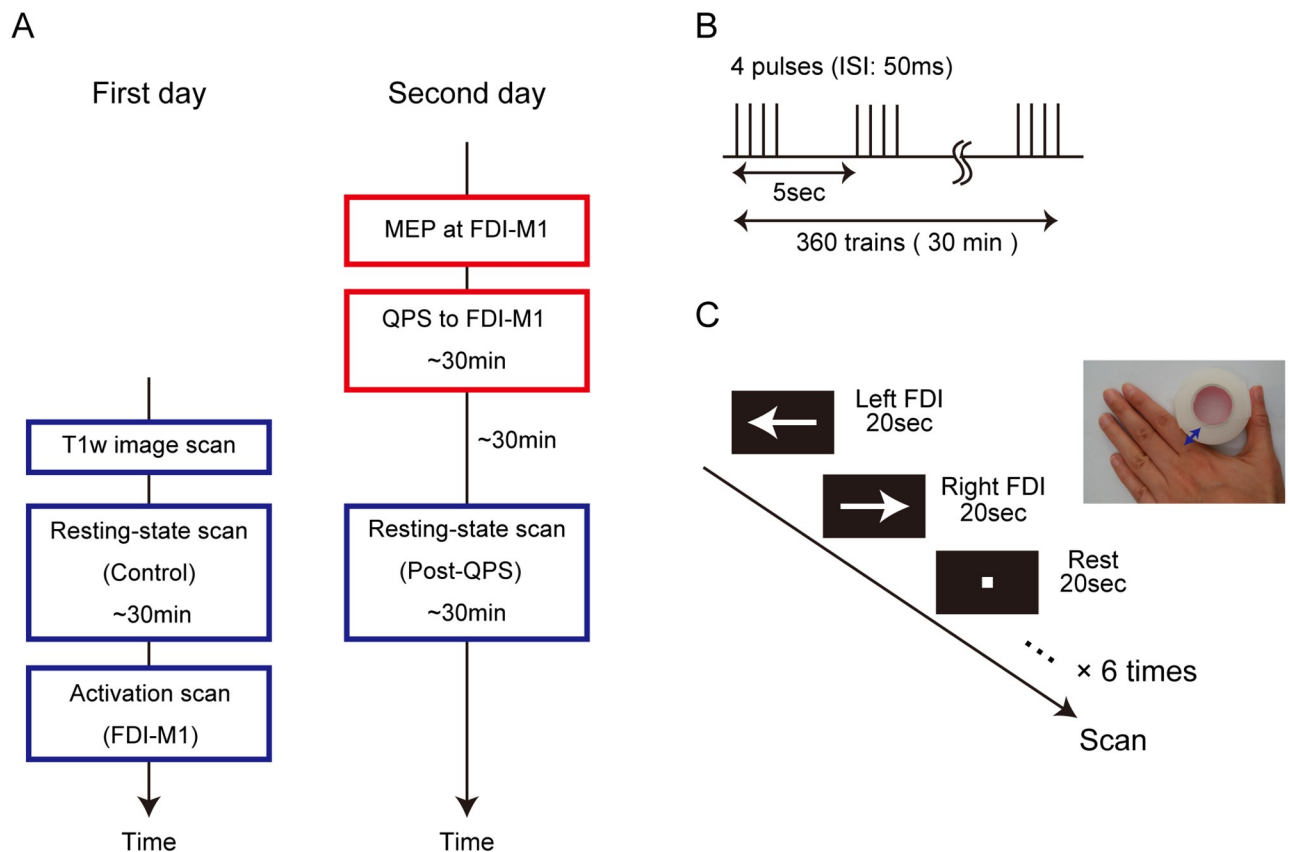


Fig 1. Overview of the experimental design. (A) On the first day, the T1-weighted image and resting-state (control) scans were obtained. On the second day, MEP after single-pulse TMS was measured to identify the FDI representation in the M1. Then, QPS was delivered to the FDI-M1 region for 30 min to induce cortical plasticity. After an approximately 30 min break, the resting-state scan (post-QPS) was administered. (B) A QPS sequence that consisted of 360 trains of quadripulse rTMS at 50 msec inter-stimulus interval (ISI) with an inter-train interval of 5 sec. (C) A finger movement task in a localizer scan to identify the M1 for the FDI. The subjects were instructed to move their left or right FDI at 2Hz as the arrows blinked for 20 sec each, followed by resting for 20 sec. The left-right-rest cycle was repeated six times.

<https://doi.org/10.1371/journal.pone.0224175.g001>

throughout the 30 min of QPS. After an approximately 30 min break (during which the subject was moved from a TMS room to an MRI scanner, placed into the scanner and administered with preparatory scans), a resting-state functional scan was administered for five runs to measure functional connectivity changes induced by QPS. A functional localizer scan was also administered for one run, where the subjects performed a motor task designed to activate the FDI-M1.

TMS procedures

TMS was administered using a hand-held figure-of-eight coil (7-cm diameter at each wing; The Magstim, Whitland, Dyfed, UK). Single-pulse TMS experiments were conducted to determine the optimal stimulation site and active motor threshold (AMT) for the right FDI muscle [33, 40, 45–48]. MEP was recorded from the right FDI muscle using Ag/AgCl sheet electrodes placed over the muscle belly (active) and the metacarpophalangeal joint of the index finger (reference). The signals were sent to an amplifier (MEG-5200, Nihon Kohden, Japan) through filters set at 150 Hz to 3 kHz. The AMT was defined as the lowest intensity that evoked a small response (>100 μV) in more than 5 of 10 consecutive trials when the subjects maintained a slight contraction of the right FDI (10% of the maximum voluntary contraction [MVC]) [33, 45–47]. MVC was calculated approximately 10 min before QPS administration.

There are many forms of rTMS that are widely used to induce neural plasticity [4, 49] including theta burst stimulation (TBS) [50], high-frequency rTMS [51] and low-frequency rTMS [52]. As the fMRI measurements took more than one hour (including moving from the TMS room to the MRI scanner, placing the subject into the scanner, performing preparatory scans, and resting-state measurements), an rTMS paradigm with aftereffects lasting over an hour was needed. QPS, the effect of which lasts approximately 90 min [45, 46], offered a suitable length of aftereffect for the present study.

Magnetic pulses of QPS were delivered by four magnetic stimulators (Magstim 200², The Magstim) connected to a specially designed combining module (The Magstim). QPS consisted of trains of four monophasic TMS pulses with an inter-train interval (ITI) of 5 sec, based on the standard protocol of QPS [45, 46, 53] (Fig 1B). Each train consisted of four magnetic pulses separated by inter-stimulus intervals (ISIs) of 50 msec (inhibitory QPS). One QPS block consisted of 360 consecutive trains that took 30 min. The intensity of QPS was set at 90% AMT and was 40.8 ± 7.0 (mean \pm SD) % of the maximum stimulator output. We did not use QPS with an ISI of 5 msec (excitatory QPS) because it is well known that facilitation is often associated with surround inhibition [54, 55]. It is well established that the inhibitory QPS reduces MEP by approximately 50% for approximately 90 min [45, 46]. The QPS effect in MEP was also confirmed in our previous study of fMRI-rTMS [33]. Furthermore, the magnitude of connectivity changes has been shown to correlate with changes in MEP [38]. Based on these literatures, we did not record MEP to confirm the effect of QPS in this study. After QPS administration, the subjects were asked if they had a headache or any other type of discomfort. No subjects reported any discomfort.

An online navigator assured that stimulation was targeted to the left FDI-M1 determined by the MEP measurements. T1-weighted images were registered to subjects' heads in space using a tracking device and navigator software (TMS Navigator-SW, Localite GmbH, Germany). The position and orientation of the coil were also registered to the subjects' heads in space and were continuously monitored and recorded in real time during QPS.

fMRI procedures

Image data were acquired using a 3-T MRI scanner and a 64-channel RF head coil (Siemens Prisma, Erlangen, Germany). T1-weighted structural images were obtained for anatomical reference (resolution = $0.8 \times 0.8 \times 0.8$ mm³). Functional images were obtained using multi-band gradient-echo echo-planar sequences [56] (TR = 1.0 sec, TE = 30 msec, flip angle = 62 deg, FOV = 192×192 mm², matrix size = 96×96 , 78 contiguous slices, voxel size = $2.0 \times 2.0 \times 2.0$ mm³, multi-band factor = 6, phase encode direction: posterior to anterior). Before each run, one functional image was acquired with opposite phase-encode direction for subsequent topup distortion correction [57].

The resting-state fMRI scan consisted of five runs of 6 min each, and the subjects were instructed to fixate on a cross during the scans. The localizer scan was also conducted to identify the M1 for the right FDI and consisted of one run of 6 min. During the FDI motor task, a left or right arrow appeared and blinked in the display, and the subjects were instructed to move their left or right FDI at 2 Hz as the arrows blinked for 20 sec each, followed by resting for 20 sec (Fig 1C). The left-right-rest cycle was repeated six times during the run.

Image analysis for resting-state data

Images were first slice timing corrected, realigned using SPM8 (www.fil.ion.ucl.ac.uk/spm/), and topup distortion corrected using FSL [58]. For topup distortion correction, the susceptibility-induced off-resonance field was estimated using images with distortions going in opposite

directions [57]. Temporal filters ($0.009 \text{ Hz} < f < 0.08 \text{ Hz}$) were applied to images using in-house-written Matlab scripts. A general linear model (GLM) [59] was used to regress out nuisance signals that correlated with head motion, whole-brain global signal, averaged ventricular signal, and averaged white matter signal. To prepare for subsequent interhemispheric functional connectivity analyses, obtained residual images were made symmetrical by spatial normalization to the MNI template and were spatially smoothed [full width at half maximum (FWHM) = 4 mm].

Then, we estimated how QPS changed the voxel-wise inter-hemispheric functional connectivity (Fig 2A). Each voxel in the left hemisphere of each subject was used as a seed to calculate its correlation with the corresponding voxel in the right hemisphere. For the corresponding voxel in the right hemisphere, the X coordinate of the voxels in the left hemisphere was flipped. A voxel-wise interhemispheric correlation was calculated for each seed voxel, and the correlation coefficient was then converted to Fisher's z [60, 61] (Fig 2B). Since the interhemispheric connectivity map is symmetrical by definition, the z values are shown only in the left hemisphere for display purposes (Fig 2A). The z -map of the post-QPS was then contrasted with that of the control scans in each subject (Fig 2B). The differential interhemispheric connectivity map was transformed back into the original space for individual analyses. For group analyses, the spatial smoothing kernel was greater (FWHM = 6 mm) than that for single subject analyses (FWHM = 4 mm), and the differential z -maps were entered into a second-level one-sample t -test, treating subjects as a random effect.

Image analysis for localizer scan data

Similarly to the analysis for resting-state data, images were first slice timing corrected, realigned, and distortion corrected using topup. The images were then spatially smoothed (FWHM = 4 mm). Time-series data were analyzed with a block design. The event timings of two types of trials (moving right/left FDI) were coded into a GLM, together with temporal and dispersion derivatives using the canonical hemodynamic response function. Six parameters of head motion derived from realignment were also included in the model as covariates of no interest. The right FDI-M1 in the left hemisphere was determined by calculating contrast images defined as moving right FDI > moving left FDI for each subject, to counterbalance non-motor components such as visual response to a cue and effort of finger movements. For group analyses, images were normalized to the template and were spatially smoothed with a greater kernel (FWHM = 6 mm), and contrast images were entered into a second-level one-sample t -test, treating subjects as a random effect.

Results

Stability of the stimulation site

To maintain spatially accurate stimulation throughout the 30-min QPS, the online navigation system was utilized. The variability of the points of stimulation was estimated to confirm the spatial extent of the stimulation site. Fig 3A shows the points of stimulation on the plane contacting the brain surface in one representative subject. One count represents the coil position during one train of four pulses. The distribution of the stimulation points in the subject group is shown in Fig 3B as a function of the distance from the center. Counts with distances between 0 to 0.25 mm from the center were normalized to 1. The half width at half maximum (HWHM), which is a half of FWHM and measures the cluster extent from its center, of the counts was approximately 0.5 mm. Most of the stimulation points ($96.0 \pm 6.0\%$, mean \pm SD) were located within a circle of 1 mm radius. The distance between the coil and the brain surface is known to be approximately 15 mm [62–65], and the variability increases as the

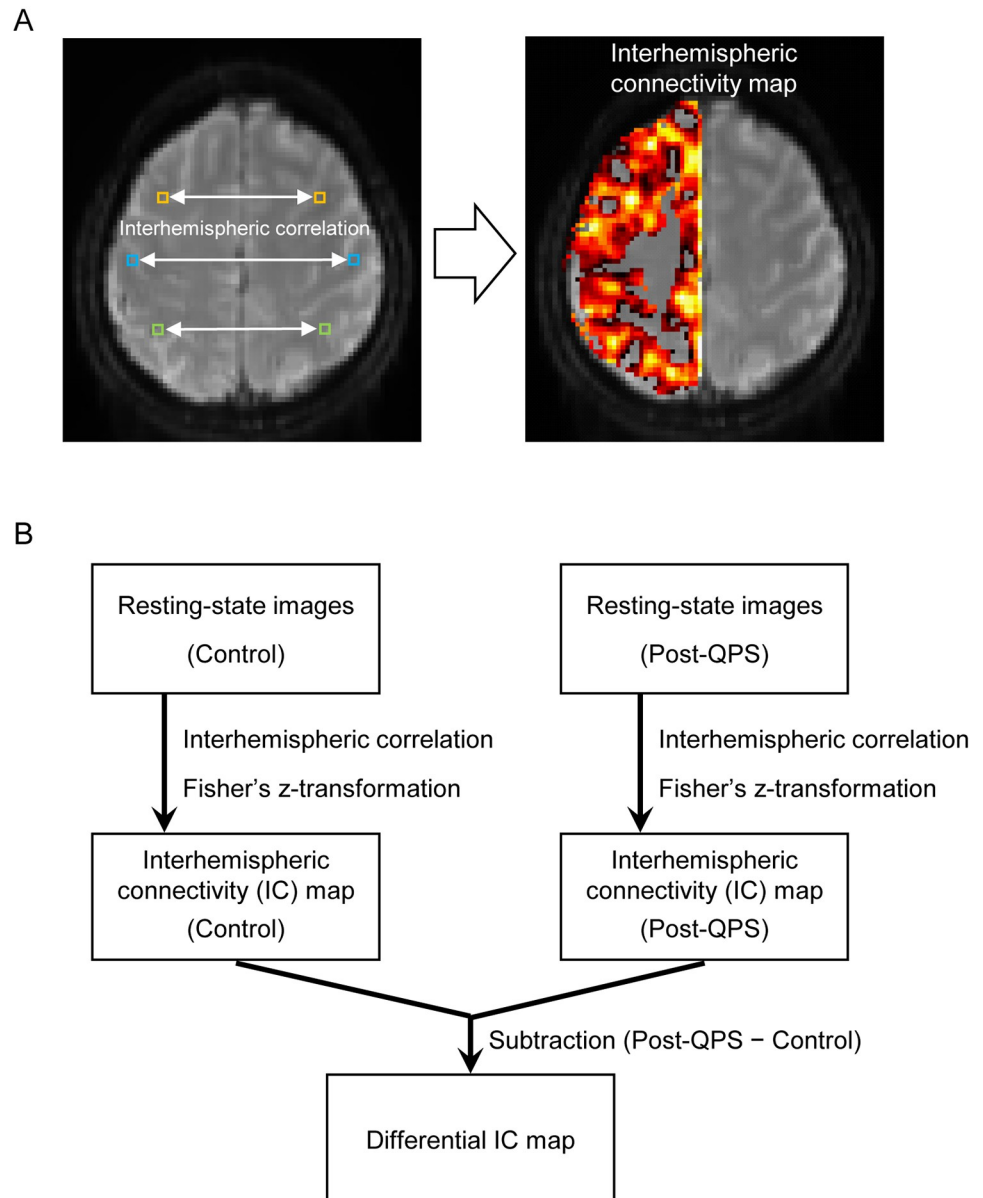


Fig 2. Interhemispheric functional connectivity analysis. (A) Each voxel in the left hemisphere of each subject was used as a seed to calculate its interhemispheric correlation with the corresponding voxel in the right hemisphere. The z values are shown only in the left hemisphere for display purposes. (B) The interhemispheric connectivity map of the post-QPS scans was calculated and was contrasted with that of the control scans to generate the differential interhemispheric connectivity map of each subject.

<https://doi.org/10.1371/journal.pone.0224175.g002>

stimulation goes deeper into the brain. However, navigation monitoring results confirmed that the stimulation site was reasonably stable compared to the size of a cluster of connectivity changes described later.

Changes in interhemispheric functional connectivity after QPS

We estimated changes in cortical plasticity by calculating the difference in interhemispheric functional connectivity between the post-QPS and control scans. Fig 4A demonstrates a cluster

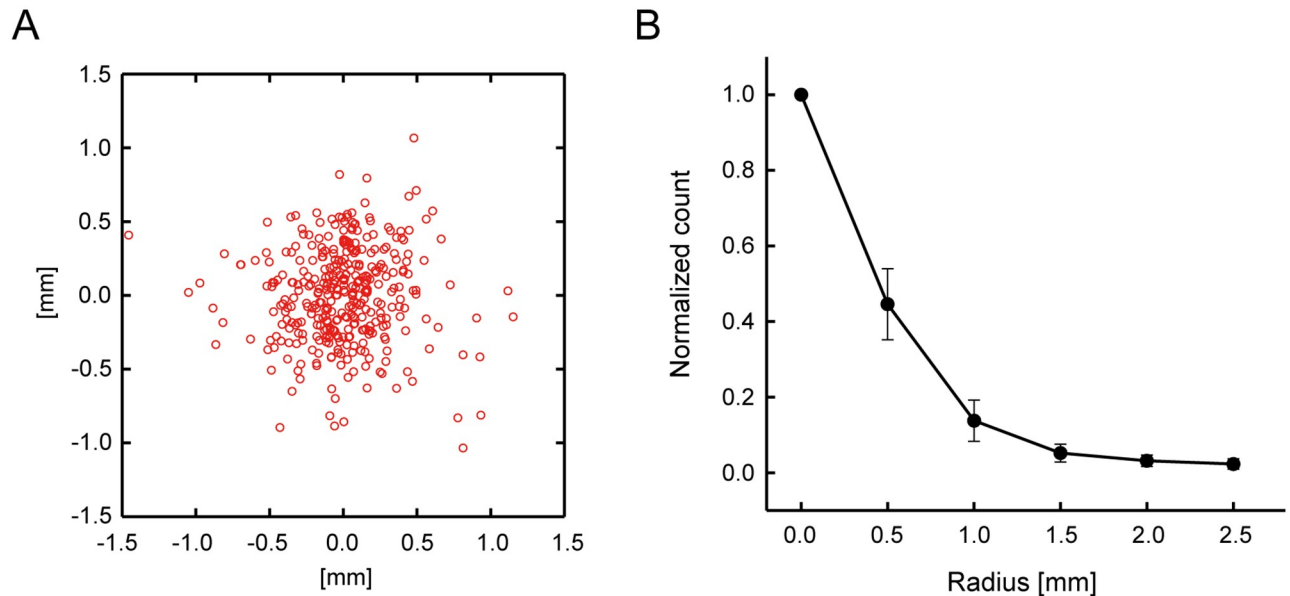


Fig 3. Monitoring of the stimulation site during QPS using an online navigation system. (A) The points of stimulation on the plane contacting the brain surface in one representative subject. Each dot represents one position of one-train stimulation. (B) The distribution of the stimulation points in the subject group as a function of the distance from the center. The counts with distances between 0 to 0.25 mm from the center were normalized to 1. The error bars indicate the standard error of means (SEM) of the subject group.

<https://doi.org/10.1371/journal.pone.0224175.g003>

of voxels with changes in the interhemispheric functional connectivity observed in the central sulcus in one representative subject. The cluster was spatially restricted around the stimulation site in the central sulcus, extending to the brain along the stimulation vector. The stimulation vector was perpendicular to the cortex as long as the experimenter stimulated the region indicated by the navigator system. Fig 4B shows the spatial extent of the cluster when the differential connectivity maps were sliced by different angles around the stimulation vector. The cluster of high connectivity changes appeared similar in spatial extent, irrespective of the different angles.

Interhemispheric functional connectivity was calculated based on the assumption that when a voxel in one hemisphere is gray matter, a voxel in the contralateral hemisphere is also gray matter. However, this is not always the case. To address this issue, interhemispheric functional connectivity was calculated between a gray matter voxel in one hemisphere and the gray matter voxel located nearest to the corresponding voxel in the contralateral hemisphere, if the corresponding voxel is judged as white matter based on the segmentation process in SPM. Fig 5 shows differential interhemispheric connectivity maps calculated in these two ways. The spatial patterns of the z values were almost the same in the central sulcus, as well as in other clusters of no interest outside the central sulcus. The results validate the differential interhemispheric connectivity pattern calculated simply between symmetrical voxels.

We then estimated how far the connectivity cluster extended in the brain surface and along the stimulation vector. Fig 6A and 6B show the differential Fisher's z of the connectivity cluster in the brain surface along the long (X) and short (Y) axes of the stimulation coil, respectively. The cluster was spatially extended approximately 10 mm from the stimulation site (HWHM: approximately 3 mm), to a significantly greater extent in the anterior than in the posterior direction along the Y axis [$t(19) = 2.2$, $P < 0.05$], reflecting the direction of magnetic field from the stimulation coil. In Fig 6C, the differential Fisher's z was plotted along the stimulation

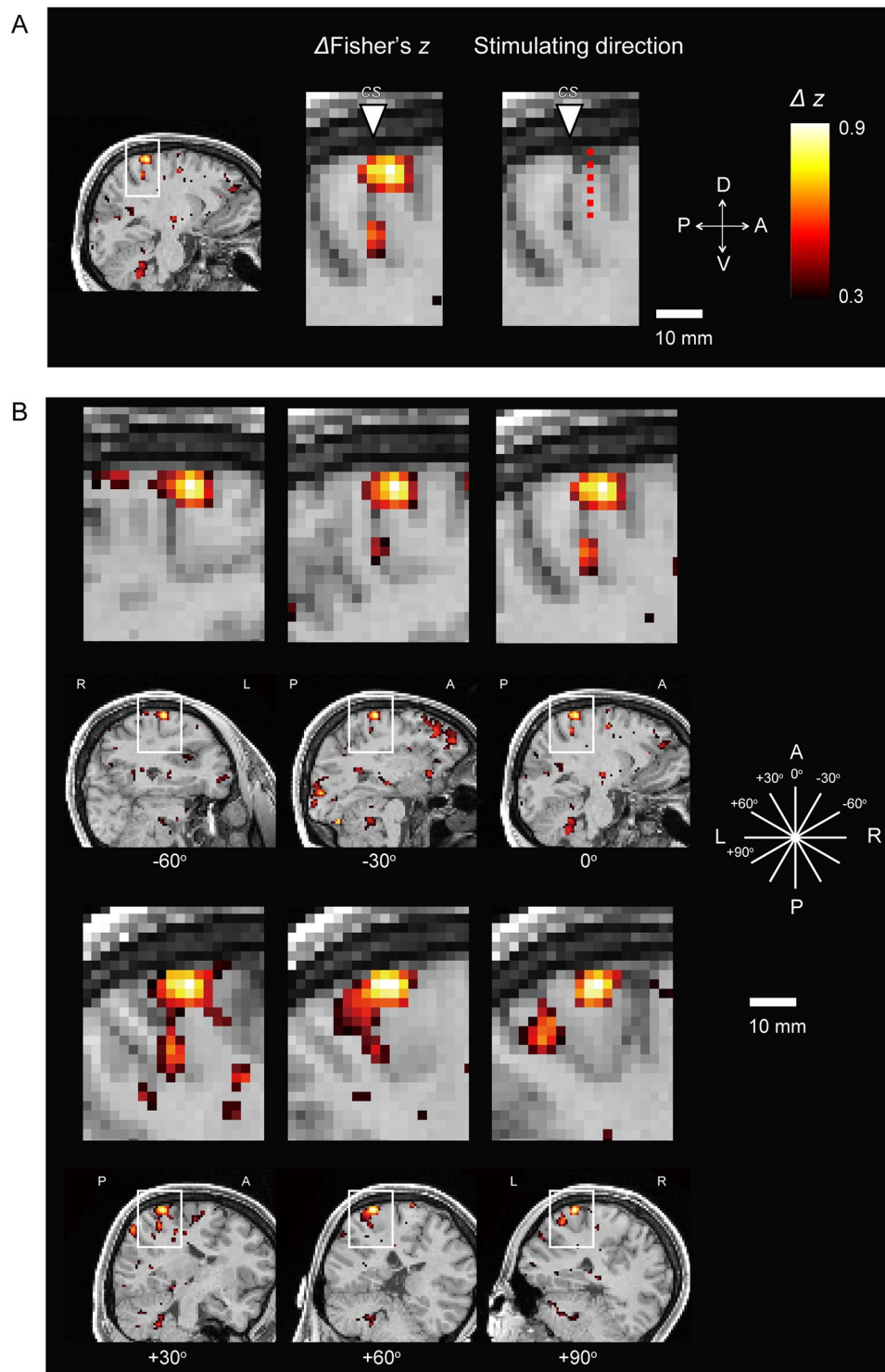


Fig 4. Differential interhemispheric connectivity map. (A) The differential interhemispheric connectivity map overlaid onto a structural image in one representative subject. The triangle indicates the central sulcus in the left hemisphere, and the red dashed line indicates the stimulation vector (the length of the vector in the figure is arbitrary). The color scale represents the differential Fisher's z value. D: dorsal, V: ventral, A: anterior, P: posterior. (B) The differential interhemispheric connectivity maps sliced by different angles around the stimulation vector. L: left, R: right.

<https://doi.org/10.1371/journal.pone.0224175.g004>

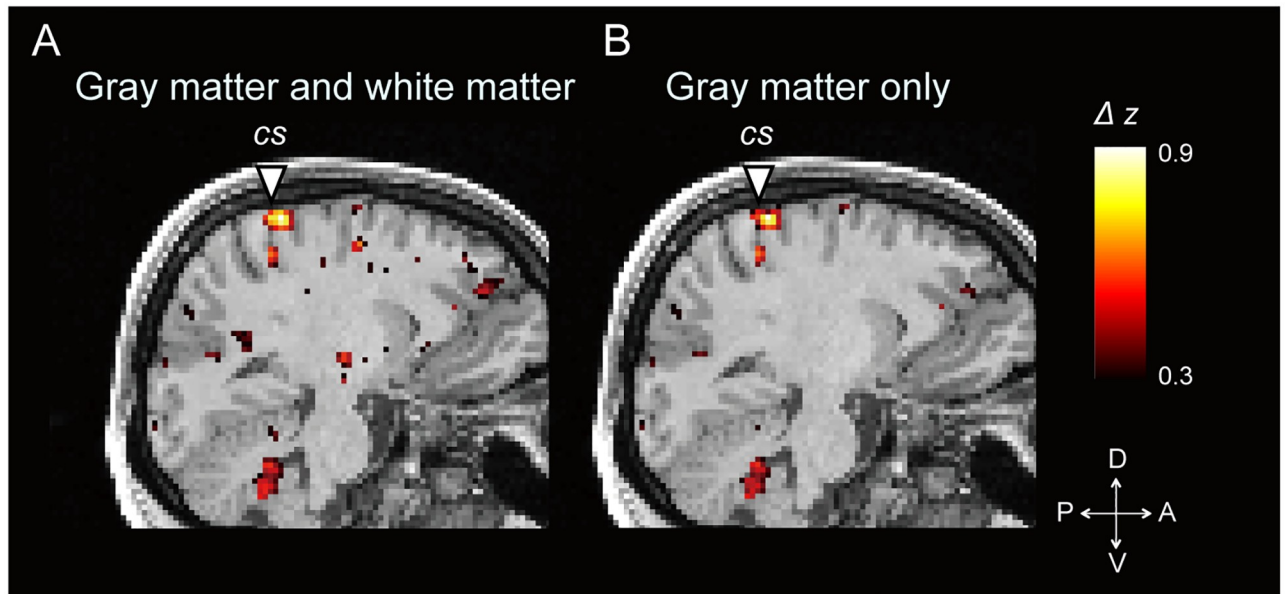


Fig 5. Two ways of calculating interhemispheric connectivity maps. (A) A differential interhemispheric connectivity map calculated simply between symmetrical voxels in the two hemispheres. Therefore, the voxel in the contralateral hemisphere can be gray matter or white matter. The map is the same as Fig 4A. (B) A differential interhemispheric connectivity map calculated in another way. The map was calculated between a gray matter voxel in one hemisphere and the gray matter voxel located nearest to the corresponding voxel in the contralateral hemisphere, if the corresponding voxel is judged as white matter.

<https://doi.org/10.1371/journal.pone.0224175.g005>

vector from the brain surface. Data in white matter voxels were excluded from group averaging. The z value gradually declined along the vector up to approximately 20 mm in depth (HWHM: approximately 7 mm). For reference, the distance from the coil and brain surface was 16.1 ± 2.9 mm (mean \pm SD). Fig 6D shows the inter-individual variability of the differential interhemispheric connectivity at the origin of the cluster ($X = 0, Y = 0, Z = 0$). There were no subjects with a negative z value. The distribution was normal (Kormogorov-Smirnov test, $P > 0.9$) (Fig 6E). These results suggest that some subjects were less sensitive but were within a normal distribution.

To examine the effect of stimulation strength (i.e., 90% AMT) on differential interhemispheric functional connectivity, correlation was calculated between the differential z score and the stimulation strength across subjects. There was no significant correlation ($r = -0.1, P > 0.05$), suggesting that stronger stimulation does not result in greater connectivity changes.

Brain activation during FDI movement

To validate differential interhemispheric connectivity maps, brain activity was measured using fMRI while the same subjects performed a motor task designed to activate the right FDI representation in the M1 in the left hemisphere. The interhemispheric connectivity difference should be greatest near the surface (Fig 6), while the brain activation peak may be not always located near the surface. Therefore, the peaks of the interhemispheric connectivity difference and brain activation will not always overlap, but the clusters of the two should spatially overlap. Fig 7A shows the differential interhemispheric connectivity map and brain activation map in one representative subject in the original subject space (see also S1 Fig). The peaks of the two maps did not overlap, but their clusters considerably overlapped, especially in the central

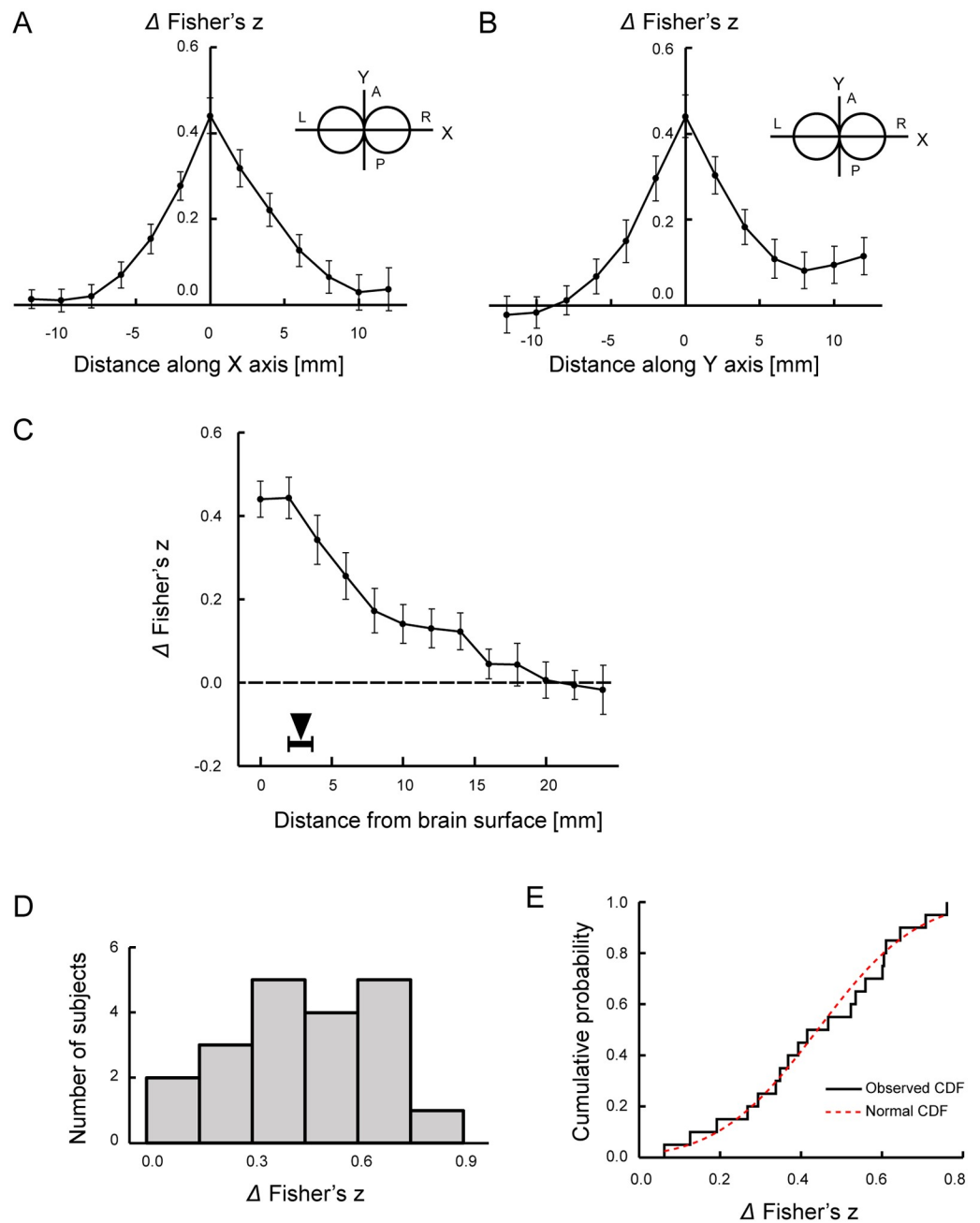


Fig 6. Cluster of connectivity changes in the surface and depth directions. (A) The differential Fisher's z plotted along the long axis (X) in the brain surface. Vertical error bars indicate the SEM of the z values. (B) The differential Fisher's z plotted along the short axis (Y) in the brain surface. (C) The differential Fisher's z plotted along the stimulation vector (Z) from the brain surface. Data in white matter voxels were excluded from group averaging. The black triangle indicates the mean depth of the activation peak in M1, and the horizontal error bar indicates the SEM of the depth of the activation peaks. (D) Distribution of differential Fisher's z in the subjects at the origin ($X = 0, Y = 0, Z = 0$) of the connectivity cluster. (E) Cumulative distribution function of the differential Fisher's z of the subjects (shown in black). A red curve indicates the case of a normal distribution.

<https://doi.org/10.1371/journal.pone.0224175.g006>

sulcus region stimulated by QPS. Fig 7B shows the group results of the two maps in MNI space (see also S1 Fig). These two maps also exhibited considerably overlapping patterns, confirming that the largest part of the cluster of connectivity changes in the central sulcus is located at the right FDI representation in the M1.

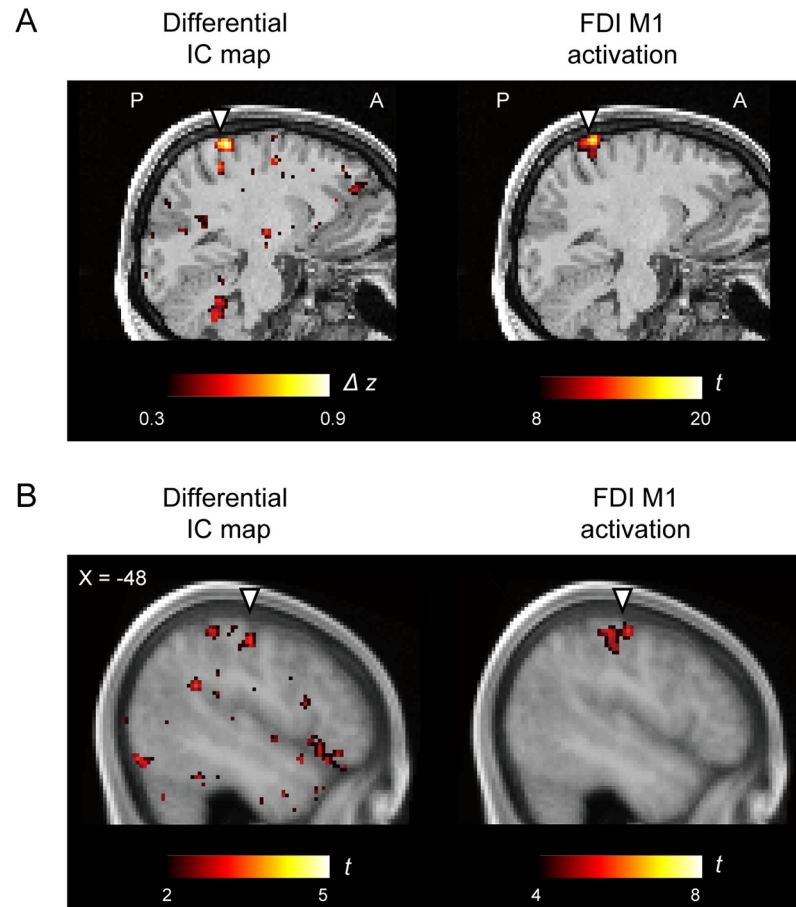


Fig 7. Comparison of differential interhemispheric connectivity and brain activity during finger movement. (A) The differential interhemispheric connectivity map (left) and brain activation map (right) in one representative subject (the same as Figs 4 and 5) in the original subject space. Triangles indicate the central sulcus of the subject. The color scale represents the differential Fisher's z value (left) or t -value (right). (B) Group results of the two maps in MNI space. Triangles indicate the central sulcus.

<https://doi.org/10.1371/journal.pone.0224175.g007>

Discussion

The present fMRI study utilized interhemispheric functional connectivity to examine the spatial extent of cortical plasticity induced in M1 by applying QPS with good spatial accuracy supported by an online navigator. A cluster of connectivity changes was observed mostly in the restricted region in the central sulcus, around a circle of 20 mm in diameter. The cluster extended in depth by approximately 20 mm. The activation related to finger movement in the left central sulcus region overlapped with the cluster of connectivity changes. These results indicate that connectivity changes in M1 were relatively restricted in space and suggest that interhemispheric functional connectivity can be used for visualization of cortical plasticity induced in the stimulated region.

Changes in interhemispheric connectivity after QPS to the left M1 were rarely seen outside the M1. Interhemispheric connectivity changes in the M1 indicate changes in connectivity between the left M1 (stimulated) and the right M1. Stimulation to the left M1 may induce changes in connectivity between the left M1 and the ipsilateral regions such as the premotor cortex. On the other hand, interhemispheric connectivity changes in the premotor cortex indicate changes in connectivity between the left premotor cortex and the right premotor cortex.

Therefore, the interhemispheric connectivity changes outside the M1 require multi-step connectivity changes, which may explain the faint interhemispheric connectivity changes outside the M1.

It must be noted that cortical plasticity estimated using interhemispheric connectivity has potential limitations. First, the stimulation of one region may lead to changes in cortical excitability in other regions, as well as deeper parts of the stimulated region, in the same brain network [22, 27, 40, 43]. Although we only observed faint effects outside the M1, interhemispheric connectivity changes may detect plasticity induced outside of the stimulated region. It is also possible that the connectivity changes in the deeper part of the stimulated region may have been induced indirectly. Second, connectivity in the stimulated region may not always change after intervention. For example, the interhemispheric connectivity did not change after 1-Hz stimulation to the inferior parietal lobule (Fig 2 in Eldaief et al., 2011 [22]). Although we have shown that QPS affected interhemispheric functional connectivity in our present and previous [33] studies, it is unclear how generally the interhemispheric connectivity can be changed in various forms of non-invasive brain stimulation. Third, structural and functional asymmetry between the left and right hemispheres exists in some brain regions, and a high degree of interhemispheric asymmetry may hinder the application of our analyses. Although it is difficult to validate the visualization in all brain regions, the present study may present one successful case in M1 with validation of visualization of cortical plasticity using brain activation during finger movement.

It is known that fatiguing muscles immediately before rTMS can evoke changes in neural activation. For example, the reductions in MEP caused by continuous TBS (cTBS) are abolished if cTBS is performed after a 2-min period of MVC [66, 67]. However, a 1-min period of MVC has been shown to not cause any lasting MEP changes [68]. In the present study, MVC was calculated approximately 10 min before QPS administration and lasted approximately only 3 sec. Therefore, the effect of MVC in this study, if any, would be excitatory and would not explain the connectivity changes induced by inhibitory QPS that we observed. However, one potential limitation would be that repeated stimulation on M1 can create lasting tingling sensations. As no control comparison was done for the sensation, it is unclear whether cutaneous changes caused by the repeated pulses affected the functional connectivity changes seen in this study.

Previous studies have estimated the electric field elicited by TMS that decays as a function of the distance from the TMS coil [5–7, 10]. The average distance between the TMS coil and the brain surface is approximately 15 mm, both in the present study and in previous studies [62–65], and the average depth of the cluster of connectivity changes was approximately 20 mm in the present study. Based on the data from previous studies on electric field measurements [5–7], the strength of the electric field in the bottom of the cluster (i.e., approximately 35 mm away from the TMS coil) decays approximately by 60 to 70% from the brain surface (i.e., approximately 15 mm away from the TMS coil), suggesting that connectivity changes can be induced by at least 30 to 40% of the electric field strength at the brain surface. The previous data of electric field measurements also suggest that connectivity changes should extend approximately 100 mm in the brain surface, where the electric field strength is almost equivalent to that at 20 mm below the center of the brain surface [6, 7]. However, connectivity changes in the gyral surface were almost restricted to 10 mm in radius in the present study, presumably because the neurons in the gyral surface are relatively less sensitive to stimulation due to the under-optimal direction of the cortical layer relative to the TMS coil [8–11].

A previous study of electroencephalography applying rTMS to the M1 reported the spatial distribution of potentiation of cortical evoked potentials outside the M1, primarily in the bilateral premotor cortex [69]. The present study examined cortical plasticity at the stimulated

region itself, the M1. It is critical to identify the spatial extent of intervention to investigate the brain-behavior relationship [70]. Visualization of the spatial extent of experimental intervention is commonly employed in animal studies, such as histological inspection of electrolytic marking for electrophysiological stimulation/recording [71–74] and intracortical virus injection for optogenetics/chemogenetics [75, 76], and visualization of intracortical drug injection using an MRI contrast agent [77, 78]. Moreover, recent advances in analyses of resting-state functional connectivity have allowed us to parcellate brain structures into numerous small functional regions [48, 79–94], highlighting the importance of accurate spatial estimation of the intervention site. The present study provides a potential way to visualize the spatial extent of intervention by rTMS in human subjects.

Supporting information

S1 Fig. Brain activation maps for a single subject and group subjects. (A) A brain activation map in one representative subject (the same as Figs 4, 5 and 7) shown in a transverse section of MNI space. Triangles indicate the central sulcus of the subject. The color scale represents t-value. The activation was present over the precentral hand knob. (B) A brain activation map of the group result.
(TIF)

Acknowledgments

We thank Ms. T. Fukui, Mr. T. Kamiya and Mr. H. Goto for technical assistance.

Author Contributions

Conceptualization: Kaori Tamura, Takahiro Osada, Seiki Konishi.

Formal analysis: Kaori Tamura, Takahiro Osada, Seiki Konishi.

Investigation: Kaori Tamura, Takahiro Osada, Akitoshi Ogawa, Masaki Tanaka, Akimitsu Suda, Yasushi Shimo, Nobutaka Hattori, Koji Kamagata, Masaaki Hori, Shigeki Aoki, Takahiro Shimizu, Hiroyuki Enomoto, Ritsuko Hanajima, Yoshikazu Ugawa.

Writing – original draft: Takahiro Osada, Seiki Konishi.

Writing – review & editing: Yoshikazu Ugawa.

References

1. Pascual-Leone A, Walsh V, Rothwell J. Transcranial magnetic stimulation in cognitive neuroscience—virtual lesion, chronometry, and functional connectivity. *Current Opinion in Neurobiology*. 2000; 10: 232–237. [https://doi.org/10.1016/s0959-4388\(00\)00081-7](https://doi.org/10.1016/s0959-4388(00)00081-7) PMID: 10753803
2. Hallett M. Transcranial magnetic stimulation: a primer. *Neuron*. 2007; 55: 187–199. <https://doi.org/10.1016/j.neuron.2007.06.026> PMID: 17640522
3. Parkin BL, Ekhtiari H, Walsh VF. Non-invasive human brain stimulation in cognitive neuroscience: a primer. *Neuron*. 2015; 87: 932–945. <https://doi.org/10.1016/j.neuron.2015.07.032> PMID: 26335641
4. Rossini PM, Burke D, Chen R, Cohen LG, Daskalakis Z, Di Iorio R, Di Lazzaro V, Ferreri F, Fitzgerald PB, George MS, Hallett M, Lefaucheur JP, Langguth B, Matsumoto H, Miniussi C, Nitsche MA, Pascual-Leone A, Paulus W, Rossi S, Rothwell JC, Siebner HR, Ugawa Y, Walsh V, Ziemann U. Non-invasive electrical and magnetic stimulation of the brain, spinal cord, roots and peripheral nerves: Basic principles and procedures for routine clinical and research application. An updated report from an I.F.C.N. Committee. *Clinical Neurophysiology*. 2015; 126: 1071–1107. <https://doi.org/10.1016/j.clinph.2015.02.001> PMID: 25797650
5. Barker AT. An introduction to the basic principles of magnetic nerve stimulation. *Journal of Clinical Neurophysiology*. 1991; 8: 26–37. PMID: 2019648

6. Jalinous R. Technical and practical aspects of magnetic nerve stimulation. *Journal of Clinical Neurophysiology*. 1991; 8: 10–25. PMID: [2019644](#)
7. Thielscher A, Kammer T. Electric field properties of two commercial figure-8 coils in TMS: calculation of focality and efficiency. *Clinical Neurophysiology*. 2004; 115: 1697–1708. <https://doi.org/10.1016/j.clinph.2004.02.019> PMID: [15203072](#)
8. Thielscher A, Opitz A, Windhoff M. Impact of the gyral geometry on the electric field induced by transcranial magnetic stimulation. *NeuroImage*. 2011; 54: 234–243. <https://doi.org/10.1016/j.neuroimage.2010.07.061> PMID: [20682353](#)
9. Opitz A, Legon W, Rowlands A, Bickel WK, Paulus W, Tyler WJ. Physiological observations validate finite element models for estimating subject-specific electric field distributions induced by transcranial magnetic stimulation of the human motor cortex. *NeuroImage*. 2013; 81: 253–264. <https://doi.org/10.1016/j.neuroimage.2013.04.067> PMID: [23644000](#)
10. Laakso I, Hirata A, Ugawa Y. Effects of coil orientation on the electric field induced by TMS over the hand motor area. *Physics in Medicine & Biology*. 2014; 59: 203–218.
11. Bungert A, Antunes A, Espenhahn S, Thielscher A. Where does TMS stimulate the motor cortex? Combining electrophysiological measurements and realistic field estimates to reveal the affected cortex position. *Cerebral Cortex*. 2017; 27: 5083–5094. <https://doi.org/10.1093/cercor/bhw292> PMID: [27664963](#)
12. Laakso I, Murakami T, Hirata A, Ugawa Y. Where and what TMS activates: experiments and modeling. *Brain Stimulation*. 2018; 11: 166–174. <https://doi.org/10.1016/j.brs.2017.09.011> PMID: [29030110](#)
13. Bestmann S, Baudewig J, Siebner HR, Rothwell JC, Frahm J. Functional MRI of the immediate impact of transcranial magnetic stimulation on cortical and subcortical motor circuits. *European Journal of Neuroscience*. 2004; 19: 1950–1962. <https://doi.org/10.1111/j.1460-9568.2004.03277.x> PMID: [15078569](#)
14. Ruff CC, Blankenburg F, Bjoertomt O, Bestmann S, Freeman E, Haynes JD, Rees G, Josephs O, Deichmann R, Driver J. Concurrent TMS-fMRI and psychophysics reveal frontal influences on human retinotopic visual cortex. *Current Biology*. 2006; 16: 1479–1488. <https://doi.org/10.1016/j.cub.2006.06.057> PMID: [16890523](#)
15. Sack AT, Kohler A, Bestmann S, Linden DE, Dechent P, Goebel R, Baudewig J. Imaging the brain activity changes underlying impaired visuospatial judgments: simultaneous fMRI, TMS, and behavioral studies. *Cerebral Cortex*. 2007; 17: 2841–2852. <https://doi.org/10.1093/cercor/bhm013> PMID: [17337745](#)
16. Driver J, Blankenburg F, Bestmann S, Vanduffel W, Ruff CC. Concurrent brain-stimulation and neuroimaging for studies of cognition. *Trends in Cognitive Sciences*. 2009; 13: 319–327. <https://doi.org/10.1016/j.tics.2009.04.007> PMID: [19540793](#)
17. Heinen K, Ruff CC, Bjoertomt O, Schenkluhn B, Bestmann S, Blankenburg F, Driver J, Chambers CD. Concurrent TMS-fMRI reveals dynamic interhemispheric influences of the right parietal cortex during exogenously cued visuospatial attention. *European Journal of Neuroscience*. 2011; 33: 991–1000. <https://doi.org/10.1111/j.1460-9568.2010.07580.x> PMID: [21324004](#)
18. Leitão J, Thielscher A, Tünnnerhoff J, Noppeney U. Concurrent TMS-fMRI reveals interactions between dorsal and ventral attentional systems. *Journal of Neuroscience*. 2015; 35: 11445–11457. <https://doi.org/10.1523/JNEUROSCI.0939-15.2015> PMID: [26269649](#)
19. Grefkes C, Nowak DA, Wang LE, Dafotakis M, Eickhoff SB, Fink GR. Modulating cortical connectivity in stroke patients by rTMS assessed with fMRI and dynamic causal modeling. *NeuroImage*. 2010; 50: 233–242. <https://doi.org/10.1016/j.neuroimage.2009.12.029> PMID: [20005962](#)
20. Schneider SA, Pleger B, Draganski B, Cordivari C, Rothwell JC, Bhatia KP, Dolan RJ. Modulatory effects of 5Hz rTMS over the primary somatosensory cortex in focal dystonia—an fMRI-TMS study. *Movement Disorders*. 2010; 25: 76–83. <https://doi.org/10.1002/mds.22825> PMID: [20058321](#)
21. Vercammen A, Knegtering H, Liemburg EJ, den Boer JA, Aleman A. Functional connectivity of the temporo-parietal region in schizophrenia: effects of rTMS treatment of auditory hallucinations. *Journal of Psychiatric Research*. 2010; 44: 725–731. <https://doi.org/10.1016/j.jpsychires.2009.12.011> PMID: [20189190](#)
22. Eldaief MC, Halko MA, Buckner RL, Pascual-Leone A. Transcranial magnetic stimulation modulates the brain's intrinsic activity in a frequency-dependent manner. *Proceedings of the National Academy of Sciences of the United States of America*. 2011; 108: 21229–21234. <https://doi.org/10.1073/pnas.1113103109> PMID: [22160708](#)
23. Fox MD, Buckner RL, White MP, Greicius MD, Pascual-Leone A. Efficacy of TMS targets for depression is related to intrinsic functional connectivity with the subgenual cingulate. *Biological Psychiatry*. 2012; 72: 595–603. <https://doi.org/10.1016/j.biopsych.2012.04.028> PMID: [22658708](#)
24. Fox MD, Halko MA, Eldaief MC, Pascual-Leone A. Measuring and manipulating brain connectivity with resting state functional connectivity magnetic resonance imaging (fcMRI) and transcranial magnetic

- stimulation (TMS). *NeuroImage*. 2012; 62: 2232–2243. <https://doi.org/10.1016/j.neuroimage.2012.03.035> PMID: 22465297
25. Bilek E, Schafer A, Ochs E, Esslinger C, Zangl M, Plichta MM, Braun U, Kirsch P, Schulze TG, Rietschel M, Meyer-Lindenberg A, Tost H. Application of high-frequency repetitive transcranial magnetic stimulation to the DLPFC alters human prefrontal-hippocampal functional interaction. *Journal of Neuroscience*. 2013; 33: 7050–7056. <https://doi.org/10.1523/JNEUROSCI.3081-12.2013> PMID: 23595762
 26. Chen AC, Oathes DJ, Chang C, Bradley T, Zhou ZW, Williams LM, Glover GH, Deisseroth K, Etkin A. Causal interactions between fronto-parietal central executive and default-mode networks in humans. *Proceedings of the National Academy of Sciences of the United States of America*. 2013; 110: 19944–19949. <https://doi.org/10.1073/pnas.1311772110> PMID: 24248372
 27. Gratton C, Lee TG, Nomura EM, D'Esposito M. The effect of theta-burst TMS on cognitive control networks measured with resting state fMRI. *Frontiers in Systems Neuroscience*. 2013; 7: 124. <https://doi.org/10.3389/fnsys.2013.00124> PMID: 24416003
 28. Rahnev D, Kok P, Munneke M, Bahdo L, de Lange FP, Lau H. Continuous theta burst transcranial magnetic stimulation reduces resting state connectivity between visual areas. *Journal of Neurophysiology*. 2013; 110: 1811–1821. <https://doi.org/10.1152/jn.00209.2013> PMID: 23883858
 29. Esslinger C, Schöler N, Sauer C, Gass D, Mier D, Braun U, Ochs E, Schulze TG, Rietschel M, Kirsch P, Meyer-Lindenberg A. Induction and quantification of prefrontal cortical network plasticity using 5 Hz rTMS and fMRI. *Human Brain Mapping*. 2014; 35: 140–151. <https://doi.org/10.1002/hbm.22165> PMID: 22965696
 30. Halko MA, Farzan F, Eldaief MC, Schmahmann JD, Pascual-Leone A. Intermittent theta-burst stimulation of the lateral cerebellum increases functional connectivity of the default network. *Journal of Neuroscience*. 2014; 34: 12049–12056. <https://doi.org/10.1523/JNEUROSCI.1776-14.2014> PMID: 25186750
 31. Pitcher D, Duchaine B, Walsh V. Combined TMS and FMRI reveal dissociable cortical pathways for dynamic and static face perception. *Current Biology*. 2014; 24: 2066–2070. <https://doi.org/10.1016/j.cub.2014.07.060> PMID: 25131678
 32. Wang JX, Rogers LM, Gross EZ, Ryals AJ, Dokucu ME, Brandstatt KL, Hermiller MS, Voss JL. Targeted enhancement of cortical-hippocampal brain networks and associative memory. *Science*. 2014; 345: 1054–1057. <https://doi.org/10.1126/science.1252900> PMID: 25170153
 33. Watanabe T, Hanajima R, Shirota Y, Ohminami S, Tsutsumi R, Terao Y, Ugawa Y, Hirose S, Miyashita Y, Konishi S, Kunimatsu A, Ohtomo K. Bidirectional effects on interhemispheric resting-state functional connectivity induced by excitatory and inhibitory repetitive transcranial magnetic stimulation. *Human Brain Mapping*. 2014; 35: 1896–1905. <https://doi.org/10.1002/hbm.22300> PMID: 23897535
 34. Andoh J, Matsushita R, Zatorre RJ. Asymmetric interhemispheric transfer in the auditory network: evidence from TMS, resting-state fMRI, and diffusion imaging. *Journal of Neuroscience*. 2015; 35: 14602–14611. <https://doi.org/10.1523/JNEUROSCI.2333-15.2015> PMID: 26511249
 35. Binney RJ, Lambon Ralph MA. Using a combination of fMRI and anterior temporal lobe rTMS to measure intrinsic and induced activation changes across the semantic cognition network. *Neuropsychologia*. 2015; 76: 170–181. <https://doi.org/10.1016/j.neuropsychologia.2014.11.009> PMID: 25448851
 36. Cocchi L, Sale MV, Lord A, Zalesky A, Breakspear M, Mattingley JB. Dissociable effects of local inhibitory and excitatory theta-burst stimulation on large-scale brain dynamics. *Journal of Neurophysiology*. 2015; 113: 3375–3385. <https://doi.org/10.1152/jn.00850.2014> PMID: 25717162
 37. Johnen VM, Neubert FX, Buch ER, Verhagen L, O'Reilly JX, Mars RB, Rushworth MF. Causal manipulation of functional connectivity in a specific neural pathway during behaviour and at rest. *Elife*. 2015; 4: e04585.
 38. Nettekoven C, Volz LJ, Leimbach M, Pool EM, Rehme AK, Eickhoff SB, Fink GR, Grefkes C. Inter-individual variability in cortical excitability and motor network connectivity following multiple blocks of rTMS. *NeuroImage*. 2015; 118: 209–218. <https://doi.org/10.1016/j.neuroimage.2015.06.004> PMID: 26052083
 39. Valchev N, Ćurčić-Blake B, Renken RJ, Avenanti A, Keysers C, Gazzola V, Maurits NM cTBS delivered to the left somatosensory cortex changes its functional connectivity during rest. *NeuroImage*. 2015; 114: 386–397. <https://doi.org/10.1016/j.neuroimage.2015.04.017> PMID: 25882754
 40. Watanabe T, Hanajima R, Shirota Y, Tsutsumi R, Shimizu T, Hayashi T, Terao Y, Ugawa Y, Katsura M, Kunimatsu A, Ohtomo K, Hirose S, Miyashita Y, Konishi S. Effects of rTMS of pre-supplementary motor area on fronto basal ganglia network activity during stop-signal task. *Journal of Neuroscience*. 2015; 35: 4813–4823. <https://doi.org/10.1523/JNEUROSCI.3761-14.2015> PMID: 25810512
 41. Rahnev D, Nee DE, Riddle J, Larson AS, D'Esposito M. Causal evidence for frontal cortex organization for perceptual decision making. *Proceedings of the National Academy of Sciences of the United States of America*. 2016; 113: 6059–6064. <https://doi.org/10.1073/pnas.1522551113> PMID: 27162349

42. Steel A, Song S, Bageac D, Knutson KM, Keisler A, Saad ZS, Gotts SJ, Wassermann EM, Wilkinson L. Shifts in connectivity during procedural learning after motor cortex stimulation: a combined transcranial magnetic stimulation/functional magnetic resonance imaging study. *Cortex*. 2016; 74: 134–148. <https://doi.org/10.1016/j.cortex.2015.10.004> PMID: 26673946
43. Balan PF, Gerits A, Mantini D, Vanduffel W. Selective TMS-induced modulation of functional connectivity correlates with changes in behavior. *NeuroImage*. 2017; 149: 361–378. <https://doi.org/10.1016/j.neuroimage.2017.01.076> PMID: 28179165
44. Hallett M, Di Iorio R, Rossini PM, Park JE, Chen R, Celnik P, Strafella AP, Matsumoto H, Ugawa Y. Contribution of transcranial magnetic stimulation to assessment of brain connectivity and networks. *Clinical Neurophysiology*. 2017; 128: 2125–2139. <https://doi.org/10.1016/j.clinph.2017.08.007> PMID: 28938143
45. Hamada M, Hanajima R, Terao Y, Arai N, Furubayashi T, Inomata-Terada S, Yugeta A, Matsumoto H, Shirota Y, Ugawa Y. Quadro-pulse stimulation is more effective than paired-pulse stimulation for plasticity induction of the human motor cortex. *Clinical Neurophysiology*, 2007; 118: 2672–2682. <https://doi.org/10.1016/j.clinph.2007.09.062> PMID: 17977788
46. Hamada M, Terao Y, Hanajima R, Shirota Y, Nakatani-Enomoto S, Furubayashi T, Matsumoto H, Ugawa Y. Bidirectional long-term motor cortical plasticity and metaplasticity induced by quadripulse transcranial magnetic stimulation. *Journal of Physiology*. 2008; 586: 3927–3947. <https://doi.org/10.1113/jphysiol.2008.152793> PMID: 18599542
47. Han S, Ogawa A, Osada T, Suda A, Tanaka M, Nanjo H, Shimo Y, Hattori N, Konishi S. More subjects are required for ventrolateral than dorsolateral prefrontal TMS because of intolerability and potential drop-out. *PLOS One*, 2019; 14: e0217826. <https://doi.org/10.1371/journal.pone.0217826> PMID: 31158248
48. Osada T, Ohta S, Ogawa A, Tanaka M, Suda A, Kamagata K, Hori M, Aoki S, Shimo Y, Hattori N, Shimizu T, Enomoto H, Hanajima R, Ugawa Y, Konishi S. An essential role of the intraparietal sulcus in response inhibition predicted by parcellation-based network. *Journal of Neuroscience*. 2019; 39: 2509–2521. <https://doi.org/10.1523/JNEUROSCI.2244-18.2019> PMID: 30692225
49. Fitzgerald PB, Fountain S, Daskalakis ZJ. A comprehensive review of the effects of rTMS on motor cortical excitability and inhibition. *Clinical Neurophysiology*. 2006; 117: 2584–2596. <https://doi.org/10.1016/j.clinph.2006.06.712> PMID: 16890483
50. Huang YZ, Edwards MJ, Rouinis E, Bhatia KP, Rothwell JC. Theta burst stimulation of the human motor cortex. *Neuron*. 2005; 45: 201–206. <https://doi.org/10.1016/j.neuron.2004.12.033> PMID: 15664172
51. Pascual-Leone A, Valls-Solé J, Wassermann EM, Hallett M. Responses to rapid-rate transcranial magnetic stimulation of the human motor cortex. *Brain*. 1994; 117: 847–858. <https://doi.org/10.1093/brain/117.4.847> PMID: 7922470
52. Chen R, Classen J, Gerloff C, Celnik P, Wassermann EM, Hallett M, Cohen LG. Depression of motor cortex excitability by low-frequency transcranial magnetic stimulation. *Neurology*. 1997; 48:1398–1403. <https://doi.org/10.1212/wnl.48.5.1398> PMID: 9153480
53. Nakamura K, Groiss SJ, Hamada M, Enomoto H, Kadowaki S, Abe M, Murakami T, Wiratman W, Chang F, Kobayashi S, Hanajima R, Terao Y, Ugawa Y. Variability in response to quadripulse stimulation of the motor cortex. *Brain Stimulation*. 2016; 9: 859–866. <https://doi.org/10.1016/j.brs.2016.01.008> PMID: 27692928
54. Dubbioso R, Raffin E, Karabanov A, Thielscher A, Siebner HR. Centre-surround organization of fast sensorimotor integration in human motor hand area. *Neuroimage*. 2017; 158: 37–47. <https://doi.org/10.1016/j.neuroimage.2017.06.063> PMID: 28669907
55. Leodori G, Thirugnanasambandam N, Conn H, Popa T, Berardelli A, Hallett M. Intracortical inhibition and surround inhibition in the motor cortex: a TMS-EEG study. *Frontiers in Neuroscience*. 2019; 13: 612. <https://doi.org/10.3389/fnins.2019.00612> PMID: 31249507
56. Feinberg DA, Moeller S, Smith SM, Auerbach E, Ramanna S, Gunther M, Glasser MF, Miller KL, Ugurbil K, Yacoub E. Multiplexed echo planar imaging for sub-second whole brain fMRI and fast diffusion imaging. *PLOS One*. 2010; 5: e15710. <https://doi.org/10.1371/journal.pone.0015710> PMID: 21187930
57. Andersson JL, Skare S, Ashburner J. How to correct susceptibility distortions in spin-echo echo-planar images: application to diffusion tensor imaging. *NeuroImage*. 2003; 20: 870–888. [https://doi.org/10.1016/S1053-8119\(03\)00336-7](https://doi.org/10.1016/S1053-8119(03)00336-7) PMID: 14568458
58. Smith SM, Jenkinson M, Woolrich MW, Beckmann CF, Behrens TE, Johansen-Berg H, Bannister PR, De Luca M, Drobnjak I, Flitney DE, Niazy RK, Saunders J, Vickers J, Zhang Y, De Stefano N, Brady JM, Matthews PM. Advances in functional and structural MR image analysis and implementation as FSL. *NeuroImage*. 2004; 23 Suppl 1: S208–219.
59. Worsley KJ, Friston KJ. Analysis of fMRI time-series revisited—again. *NeuroImage*. 1995; 2: 173–181. <https://doi.org/10.1006/nimg.1995.1023> PMID: 9343600

60. Fox MD, Snyder AZ, Vincent JL, Corbetta M, Van Essen DC, Raichle ME. The human brain is intrinsically organized into dynamic, anticorrelated functional networks. *Proceedings of the National Academy of Sciences of the United States of America*. 2005; 102: 9673–9678. <https://doi.org/10.1073/pnas.0504136102> PMID: 15976020
61. Fair DA, Dosenbach NU, Church JA, Cohen AL, Brahmbhatt S, Miezin FM, Barch DM, Raichle ME, Petersen SE, Schlaggar BL. Development of distinct control networks through segregation and integration. *Proceedings of the National Academy of Sciences of the United States of America*. 2007; 104: 13507–13512. <https://doi.org/10.1073/pnas.0705843104> PMID: 17679691
62. Stokes MG, Chambers CD, Gould IC, Henderson TR, Janko NE, Allen NB, Mattingley JB. Simple metric for scaling motor threshold based on scalp-cortex distance: application to studies using transcranial magnetic stimulation. *Journal of Neurophysiology*. 2005; 94: 4520–4527. <https://doi.org/10.1152/jn.00067.2005> PMID: 16135552
63. Stokes MG, Chambers CD, Gould IC, English T, McNaught E, McDonald O, Mattingley JB. Distance-adjusted motor threshold for transcranial magnetic stimulation. *Clinical Neurophysiology*. 2007; 118: 1617–1625. <https://doi.org/10.1016/j.clinph.2007.04.004> PMID: 17524764
64. Cai W, George JS, Chambers CD, Stokes MG, Verbruggen F, Aron AR. Stimulating deep cortical structures with the batwing coil: how to determine the intensity for transcranial magnetic stimulation using coil-cortex distance. *Journal of Neuroscience Methods*. 2012; 204: 238–241. <https://doi.org/10.1016/j.jneumeth.2011.11.020> PMID: 22138632
65. Cai W, George JS, Verbruggen F, Chambers CD, Aron AR. The role of the right presupplementary motor area in stopping action: two studies with event-related transcranial magnetic stimulation. *Journal of Neurophysiology*. 2012; 108: 380–389. <https://doi.org/10.1152/jn.00132.2012> PMID: 22514296
66. Iezzi E, Conte A, Suppa A, Agostino R, Dinapoli L, Scontrini A, Berardelli A. Phasic voluntary movements reverse the aftereffects of subsequent theta-burst stimulation in humans. *Journal of Neurophysiology*. 2008; 100: 2070–2076. <https://doi.org/10.1152/jn.90521.2008> PMID: 18753328
67. Goldsworthy MR, Müller-Dahlhaus F, Ridding MC, Ziemann U. Inter-subject variability of LTD-like plasticity in human motor cortex: a matter of preceding motor activation. *Brain Stimulation*. 2014; 7: 864–870. <https://doi.org/10.1016/j.brs.2014.08.004> PMID: 25216649
68. Kadowaki S, Enomoto H, Murakami T, Nakatani-Enomoto S, Kobayashi S, Ugawa Y. Influence of phasic muscle contraction upon the quadripulse stimulation (QPS) aftereffects. *Clinical Neurophysiology*. 2016; 127: 1568–1573. <https://doi.org/10.1016/j.clinph.2015.10.063> PMID: 26702773
69. Esser SK, Huber R, Massimini M, Peterson MJ, Ferrarelli F, Tononi G. A direct demonstration of cortical LTP in humans: a combined TMS/EEG study. *Brain Research Bulletin*. 2006; 69: 86–94. <https://doi.org/10.1016/j.brainresbull.2005.11.003> PMID: 16464689
70. Miyashita Y. The cutting edge in brain science and sportology. *Juntendo Medical Journal*. 2016; 62: 6–11.
71. Hubel DH, Wiesel TN. Receptive fields, binocular interaction and functional architecture in the cat's visual cortex. *Journal of Physiology*, 1962; 160: 106–154. <https://doi.org/10.1113/jphysiol.1962.sp006837> PMID: 14449617
72. Bruce CJ, Goldberg ME. Primate frontal eye fields. I. Single neurons discharging before saccades. *Journal of Neurophysiology*. 1985; 53: 603–35. <https://doi.org/10.1152/jn.1985.53.3.603> PMID: 3981231
73. Salzman CD, Murasugi CM, Britten KH, Newsome WT. Microstimulation in visual area MT: effects on direction discrimination performance. *Journal of Neuroscience*. 1992; 12: 2331–2355. PMID: 1607944
74. Koyano KW, Takeda M, Matsui T, Hirabayashi T, Ohashi Y, Miyashita Y. Laminar module cascade from layer 5 to 6 implementing cue-to-target conversion for object memory retrieval in the primate temporal cortex. *Neuron*. 2016; 92: 518–529. <https://doi.org/10.1016/j.neuron.2016.09.024> PMID: 27720482
75. Tye KM, Deisseroth K. Optogenetic investigation of neural circuits underlying brain disease in animal models. *Nature Reviews Neuroscience*. 2012; 13: 251–266. <https://doi.org/10.1038/nrn3171> PMID: 22430017
76. Sternson SM, Roth BL. Chemogenetic tools to interrogate brain functions. *Annual Reviews of Neuroscience*. 2014; 37: 387–407.
77. Hwang EJ, Hauschild M, Wilke M, Andersen RA. Inactivation of the parietal reach region causes optic ataxia, impairing reaches but not saccades. *Neuron*. 2012; 76: 1021–1029. <https://doi.org/10.1016/j.neuron.2012.10.030> PMID: 23217749
78. Miyamoto K, Osada T, Setsuie R, Takeda M, Tamura K, Adachi Y, Miyashita Y. Causal neural network of metamemory for retrospection in primates. *Science*. 2017; 355: 188–193. <https://doi.org/10.1126/science.aal0162> PMID: 28082592
79. Biswal BB, Mennes M, Zuo XN, Gohel S, Kelly C, Smith SM, Beckmann CF, Adelstein JS, Buckner RL, Colcombe S, Dogonowski AM, Ernst M, Fair D, Hampson M, Hoptman MJ, Hyde JS, Kiviniemi VJ,

- Kotter R, Li SJ, Lin CP, Lowe MJ, Mackay C, Madden DJ, Madsen KH, Margulies DS, Mayberg HS, McMahon K, Monk CS, Mostofsky SH, Nagel BJ, Pekar JJ, Peltier SJ, Petersen SE, Riedl V, Rombouts SA, Rypma B, Schlaggar BL, Schmidt S, Seidler RD, Siegle GJ, Sorg C, Teng GJ, Veijola J, Villringer A, Walter M, Wang L, Weng XC, Whitfield-Gabrieli S, Williamson P, Windischberger C, Zang YF, Zhang HY, Castellanos FX, Milham MP. Toward discovery science of human brain function. *Proceedings of the National Academy of Sciences of the United States of America*. 2010; 107: 4734–4739. <https://doi.org/10.1073/pnas.0911855107> PMID: 20176931
80. Mars RB, Sallet J, Schuffelgen U, Jbabdi S, Toni I, Rushworth MF. Connectivity-based subdivisions of the human right "temporoparietal junction area": evidence for different areas participating in different cortical networks. *Cerebral Cortex*. 2012; 22: 1894–1903. <https://doi.org/10.1093/cercor/bhr268> PMID: 21955921
 81. Zhang S, Li CS. Functional connectivity mapping of the human precuneus by resting state fMRI. *NeuroImage*. 2012; 59: 3548–3562. <https://doi.org/10.1016/j.neuroimage.2011.11.023> PMID: 22116037
 82. Zhang S, Ide JS, Li CS. Resting-state functional connectivity of the medial superior frontal cortex. *Cerebral Cortex*. 2012; 22: 99–111. <https://doi.org/10.1093/cercor/bhr088> PMID: 21572088
 83. Hirose S, Watanabe T, Wada H, Imai Y, Machida T, Shirouzu I, Miyashita Y, Konishi S. Functional relevance of micromodules in the human association cortex delineated with high-resolution FMRI. *Cerebral Cortex*. 2013; 23: 2863–2871. <https://doi.org/10.1093/cercor/bhs268> PMID: 22941719
 84. Cai W, Ryali S, Chen T, Li CS, Menon V. Dissociable roles of right inferior frontal cortex and anterior insula in inhibitory control: evidence from intrinsic and task-related functional parcellation, connectivity, and response profile analyses across multiple datasets. *Journal of Neuroscience*. 2014; 34: 14652–14667. <https://doi.org/10.1523/JNEUROSCI.3048-14.2014> PMID: 25355218
 85. Laumann TO, Gordon EM, Adeyemo B, Snyder AZ, Joo SJ, Chen MY, Gilmore AW, McDermott KB, Nelson SM, Dosenbach NU, Schlaggar BL, Mumford JA, Poldrack RA, Petersen SE. Functional system and areal organization of a highly sampled individual human brain. *Neuron*. 2015; 87: 657–670. <https://doi.org/10.1016/j.neuron.2015.06.037> PMID: 26212711
 86. Poldrack RA, Laumann TO, Koyejo O, Gregory B, Hover A, Chen MY, Gorgolewski KJ, Luci J, Joo SJ, Boyd RL, Hunicke-Smith S, Simpson ZB, Caven T, Sochat V, Shine JM, Gordon E, Snyder AZ, Adeyemo B, Petersen SE, Glahn DC, Reese Mckay D, Curran JE, Goring HH, Carless MA, Blangero J, Dougherty R, Leemans A, Handwerker DA, Frick L, Marcotte EM, Mumford JA. Long-term neural and physiological phenotyping of a single human. *Nature Communications*. 2015; 6: 8885. <https://doi.org/10.1038/ncomms9885> PMID: 26648521
 87. Wang D, Buckner RL, Fox MD, Holt DJ, Holmes A, Stoecklein S, Langs G, Pan R, Qian T, Li K, Baker JT, Stufflebeam SM, Wang K, Wang X, Hong B, Liu H. Parcellating cortical functional networks in individuals. *Nature Neuroscience*. 2015; 18: 1853–1860. <https://doi.org/10.1038/nn.4164> PMID: 26551545
 88. Eickhoff SB, Laird AR, Fox PT, Bzdok D, Hensel L. Functional segregation of the human dorsomedial prefrontal cortex. *Cerebral Cortex*. 2016; 26: 304–321. <https://doi.org/10.1093/cercor/bhu250> PMID: 25331597
 89. Glasser MF, Coalson TS, Robinson EC, Hacker CD, Harwell J, Yacoub E, Ugurbil K, Andersson J, Beckmann CF, Jenkinson M, Smith SM, Van Essen DC. A multi-modal parcellation of human cerebral cortex. *Nature*. 2016; 536: 171–178. <https://doi.org/10.1038/nature18933> PMID: 27437579
 90. Hirose S, Osada T, Ogawa A, Tanaka M, Wada H, Yoshizawa Y, Imai Y, Machida T, Akahane M, Shirouzu I, Konishi S. Lateral-medial dissociation in orbitofrontal cortex-hypothalamus connectivity. *Frontiers in Human Neuroscience*. 2016; 10: 244. <https://doi.org/10.3389/fnhum.2016.00244> PMID: 27303281
 91. Gordon EM, Laumann TO, Gilmore AW, Newbold DJ, Greene DJ, Berg JJ, Ortega M, Hoyt-Drazen C, Gratton C, Sun H, Hampton JM, Coalson RS, Nguyen AL, McDermott KB, Shimony JS, Snyder AZ, Schlaggar BL, Petersen SE, Nelson SM, Dosenbach NUF. Precision functional mapping of individual human brains. *Neuron*. 2017; 95: 791–807. <https://doi.org/10.1016/j.neuron.2017.07.011> PMID: 28757305
 92. Osada T, Suzuki R, Ogawa A, Tanaka M, Hori M, Aoki S, Tamura Y, Watada H, Kawamori R, Konishi S. Functional subdivisions of the hypothalamus using areal parcellation and their signal changes related to glucose metabolism. *NeuroImage*. 2017; 162: 1–12. <https://doi.org/10.1016/j.neuroimage.2017.08.056> PMID: 28844890
 93. Eickhoff SB, Yeo BTT, Genon S. Imaging-based parcellations of the human brain. *Nature Reviews in Neuroscience*. 2018; 19: 672–686. <https://doi.org/10.1038/s41583-018-0071-7> PMID: 30305712
 94. Ogawa A, Osada T, Tanaka M, Hori M, Aoki S, Nikolaidis A, Milham MP, Konishi S. Striatal subdivisions that coherently interact with multiple cerebrocortical networks. *Human Brain Mapping*. 2018; 39: 4349–4359. <https://doi.org/10.1002/hbm.24275> PMID: 29975005